SUPPLEMETARY INFORMATION FOR: A Minimal Mechanosensing Model Predicts Keratocyte Evolution on Flexible Substrates

Zhiwen Zhang[1], Phoebus Rosakis[2,3,*], Thomas Y. Hou[4], and Guruswami Ravichandran[5]

[1]Department of Mathematics, The University of Hong Kong, Pokfulam Road, Hong Kong SAR. Email: zhangzw@hku.hk
[2]Department of Mathematics and Applied Mathematics, University of Crete, Heraklion 70013 Crete, Greece. Email: rosakis@uoc.gr
[3]Institute of Applied and Computational Mathematics, Foundation for Research and Technology-Hellas, Voutes 70013 Crete, Greece
[4]Computing and Mathematical Sciences, California Institute of Technology, Pasadena, CA 91125, USA. Email:hou@cms.caltech.edu
[5]Division of Engineering and Applied Science, California Institute of Technology, Pasadena, CA 91125, USA. Email: ravi@caltech.edu

Supplementary Information

Plane stress

The substrate is modelled as a thin elastic plate subject to tractions from the cell that are assumed to be in-plane only, as in [S1]. Using Cartesian coordinates (x_1, x_2, x_3), the substrate midplane is the surface $x_3 = 0$, while for the plate $-h/2 \leq x_3 \leq h/2$, where h is the plate thickness. If $T_{ij}(x_1, x_2, x_3)$ are the stress components, the boundary conditions at the bottom and top surfaces are, respectively

$$T_{3\alpha}(x_1, x_2, -h/2) = 0, \quad T_{3\alpha}(x_1, x_2, h/2) = b_\alpha(x_1, x_2), \quad \alpha = 1, 2, \tag{S1}$$

where b_α are the components of the traction $\boldsymbol{b}(\boldsymbol{x}, t)$ exerted by the cell onto the substrate at a fixed time t, and it is assumed that T_{33} vanishes everywhere. We do not assume that the thickness h

vanishes. Instead, we define the thickness-resultant stresses, or two-dimentional stresses

$$S_{ij}(x_1, x_2) = \int_{-h/2}^{h/2} T_{ij}(x_1, x_2, x_3) dx_3 \tag{S2}$$

Then writing the first two 3D equilibrium equations $\sum_{j=1}^{3} \partial T_{\alpha j}/\partial x_j = 0$ (for $\alpha = 1, 2$) as

$$\sum_{\beta=1}^{2} \frac{\partial T_{\alpha\beta}}{\partial x_\beta}(x_1, x_2, x_3) + \frac{\partial T_{\alpha 3}}{\partial x_3}(x_1, x_2, x_3) = 0,$$

integrating them with respect to x_3 over the thickness (from $-h/2$ to $h/2$), and using (S1) for the integral of the second term above, we find from (S2)

$$\sum_{\beta=1}^{2} \partial S_{\alpha\beta}(x_1, x_2)/\partial x_\beta + b_\alpha(x_1, x_2) = 0$$

Letting $\boldsymbol{x} = (x_1, x_2)$, this is identical to $\nabla \cdot \boldsymbol{S}(\boldsymbol{x}, t) + \boldsymbol{b}(\boldsymbol{x}, t) = \boldsymbol{0}$. In this 2D equation, the surface traction $\boldsymbol{b}(\boldsymbol{x}, t)$ plays the role of a forcing term known as a body force in solid mechanics. Next we integrate the three-dimensional stress-strain relations over the thickness, define 2D displacements

$$u_\alpha(x_1, x_2) = (1/h) \int_{-h/2}^{h/2} U_\alpha(x_1, x_2, x_3) dx_3, \qquad \alpha = 1, 2,$$

as the thickness averages of the 3D displacements $U_\alpha(x_1, x_2, x_3)$, use the ansatz $T_{33} = 0$, and (S2) to find the two-dimensional stress-strain relations for plane stress (i.e. Eq.(1) in our paper), where

$$\bar{\lambda} = h \frac{2\lambda\mu}{\lambda + 2\mu}, \qquad \bar{\mu} = h\mu \tag{S3}$$

are the surface Lamé Moduli for plane stress [S1], expressed in terms of the 3D Lamé Moduli λ and μ, and substrate thickness h. The plane stress approximation reduces the problem to a two-dimensional problem without assuming zero thickness. In the 2D elasticity setting, stress $\boldsymbol{S}$ has units of force per unit length (one dimensional area) and body force $\boldsymbol{b}$ has units of force per unit area (two dimensional volume), as it equals 3D surface traction.

Level Set Formulation

We use the level set method [S2] which has been successfully applied to cell evolution study, e.g., [S3, S4] to solve a regularised version of the equations of the model. The regularisation allows us to extend fields defined only on the moving surface C_t to the entire domain. Let $D = [-L, L]^2 \subset \mathbb{R}^2$ be the region occupied by the substrate, with the cell $\Omega_t \subset D$. For $\varepsilon > 0$ a small parameter, let H_ε be the (smooth) *regularised step function*, so that

$$H_\varepsilon'(z) > 0 \quad \text{for } |z| < \varepsilon, \qquad H_\varepsilon(z) = \begin{cases} 1, & z \geq \varepsilon, \\ 0, & z \leq -\varepsilon. \end{cases}$$

Its derivative, the *regularised delta function* δ_ε has support $[-z, z]$ and satisfies

$$\delta_\varepsilon(z) = H'_\varepsilon(z), \qquad \int_{-\varepsilon}^{\varepsilon} \delta_\varepsilon(z)dz = 1$$

The *level set function* $\varphi(\boldsymbol{x}, t)$ vanishes on C_t, is positive inside Ω_t and negative outside it. It evolves according to the *level set equation*

$$\varphi_t - V_n|\nabla\varphi| = 0 \quad \text{in } D \tag{S4}$$

where $V_n = V_n(\boldsymbol{x}, t)$ is the normal velocity of the level set of φ through $\boldsymbol{x}$ at time t. The characteristic function is thus $\chi_{\Omega_t}(\boldsymbol{x}, t) = H(\varphi(\boldsymbol{x}, t))$, where H is the usual Heaviside step function. In the regularised scheme χ_{Ω_t} is replaced by the *regularised characteristic function*

$$H_\varepsilon(\varphi(\boldsymbol{x}, t))$$

for $\boldsymbol{x} \in D$. The regularised cell centroid and corresponding velocity are thus

$$\bar{\boldsymbol{x}}_\varepsilon(t) = \frac{\int_D \boldsymbol{x} H_\varepsilon(\varphi(\boldsymbol{x}, t))d\boldsymbol{x}}{\int_D H_\varepsilon(\varphi(\boldsymbol{x}, t))d\boldsymbol{x}}, \quad \bar{\boldsymbol{v}}_\varepsilon = \dot{\bar{\boldsymbol{x}}}_\varepsilon \tag{S5}$$

see Eq.(4) in our paper. The *regularised body force* is

$$\boldsymbol{b}_\varepsilon(\boldsymbol{x}, t) = -K(\boldsymbol{I} + e\bar{\boldsymbol{v}}_\varepsilon \otimes \bar{\boldsymbol{v}}_\varepsilon)(\boldsymbol{x} - \bar{\boldsymbol{x}}_\varepsilon)H_\varepsilon(\varphi(\boldsymbol{x}, t)), \quad \boldsymbol{x} \in D \tag{S6}$$

Accordingly, the regularised version of the Eq.(9) in our paper is $\nabla \cdot \boldsymbol{S} + \boldsymbol{b}_\varepsilon = \boldsymbol{0}$ in D, or

$$\mu\Delta\boldsymbol{u} + (\lambda + \mu)\nabla(\nabla\cdot\boldsymbol{u}) + \boldsymbol{b}_\varepsilon(\boldsymbol{x}, t) = \boldsymbol{0} \quad \text{in } D \tag{S7}$$

in view of Eqs.(1) and (9) in our paper. Define the unit normal field

$$\boldsymbol{n}(\boldsymbol{x}, t) = -\frac{\nabla\varphi(\boldsymbol{x}, t)}{|\nabla\varphi(\boldsymbol{x}, t)|}, \quad \boldsymbol{x} \in D \tag{S8}$$

and the regularised normal velocity as in the Eq.(10) of our paper with $\boldsymbol{v}_{s\varepsilon} = (1/\zeta)\boldsymbol{b}_\varepsilon$ in place of $\boldsymbol{v}_s$:

$$V_{n\varepsilon} = -\gamma(\boldsymbol{I} + e\bar{\boldsymbol{v}}_\varepsilon \otimes \bar{\boldsymbol{v}}_\varepsilon)(\boldsymbol{x} - \bar{\boldsymbol{x}}_\varepsilon)\cdot\boldsymbol{n} + G(\boldsymbol{n}\cdot\boldsymbol{S}\boldsymbol{n}), \quad \text{in } D \tag{S9}$$

where

$$\boldsymbol{n}\cdot\boldsymbol{S}\boldsymbol{n} = \frac{1}{|\nabla\varphi|^2}\nabla\varphi\cdot\boldsymbol{S}\nabla\varphi. \tag{S10}$$

Here we have used the Eq.(S8) above and Eq.(1) in our paper. The Hamilton-Jacobi equation

$$\varphi_t - V_{n\varepsilon}|\nabla\varphi| = 0 \quad \text{in } D \tag{S11}$$

governs the evolution of the level set function. The regularised problem is to find $(\boldsymbol{u}, \varphi)$ satisfying Eqs. (S7) and (S11) subject to initial conditions specifying the initial cell domain $\Omega_0 \subset D$, $\boldsymbol{u}(\cdot, 0) = \boldsymbol{0}$, $\varphi(\boldsymbol{x}, 0) = \pm\text{dist}(\partial\Omega, \boldsymbol{x})$ with the $+$ choice inside $\partial\Omega$ and the $-$ choice outside (signed distance form $\partial\Omega$), and suitable boundary conditions on ∂D. Then the cell boundary C_t is the zero level set of $\varphi(\cdot, t)$. with $V_{n\varepsilon}$ given by (S9) and $\boldsymbol{S}$ by Eq.(1) in our paper.

Finite difference discretisation

Discretisation of the displacement field

We use finite difference method to discretize the regularised model (level-set formulation) developed in the previous section. First, we specify regularised version of the singular Dirac delta function δ and the discontinuous Heaviside function H. In our numerical discretisations, we define the regularised delta function as δ_ε as

$$\delta_\varepsilon(x) = \begin{cases} \frac{1}{2}(1+\cos(\pi x/\varepsilon))/\varepsilon, & |x| < \varepsilon \\ 0, & |x| \geq \varepsilon \end{cases} \tag{S12}$$

and the corresponding regularised Heaviside function H_ε is defined as

$$H_\varepsilon(x) = \begin{cases} 0, & x < -\varepsilon \\ (x+\varepsilon)/(2\varepsilon) + \sin(\pi x/\varepsilon))/(2\pi), & |x| < \varepsilon \\ 1, & x > \varepsilon \end{cases} \tag{S13}$$

We have the relation $H'_\varepsilon(x) = \delta_\varepsilon(x)$.

We partition the domain $D = [-L_x, L_x] \times [-L_y, L_y]$ into $(N_x+1) \times (N_y+1)$ grids (x_i, y_j) with $x_i = (i-1)h - L_x$, $y_j = (j-1)h - L_y$, $1 \leq i \leq N_x+1$, $1 \leq j \leq N_y+1$ and mesh $h = \frac{2L_x}{N_x} = \frac{2L_y}{N_y}$. Recall that $\mathbf{u} = (u, v)^T$. Denote by $u^n_{i,j}$ the approximation of $u(x_i, y_j, t_n)$, where $t_n = n\Delta t$, Δt is the time step, and n is a nonnegative integer. The approximations to $v(x_i, y_j, t_n)$ and $\varphi(x_i, y_j, t_n)$ can be defined in the same fashion. For the discretisation in space, we use a second-order, centered-difference scheme. We introduce the finite difference operators

$$\begin{aligned} D^x_0 f_{i,j} &= (f_{i+1,j} - f_{i-1,j})/2h, && \text{(central difference)}, \\ D^x_- f_{i,j} &= (f_{i,j} - f_{i-1,j})/2h, && \text{(backward difference)}, \\ D^x_+ f_{i,j} &= (f_{i+1,j} - f_{i,j})/2h, && \text{(forward difference)}. \end{aligned}$$

The operators D^y_0, D^y_-, and D^y_+ are defined similarly. If we write in element-wise form, the regularised PDE of the displacement field satisfies,

$$(\lambda+2\mu)u_{xx} + (\lambda+\mu)v_{xy} + \mu u_{yy} = KH_\varepsilon(\varphi)(x - \bar{x}_\varepsilon), \tag{S14}$$

$$\mu v_{xx} + (\lambda+\mu)u_{xy} + (\lambda+2\mu)v_{yy} = KH_\varepsilon(\varphi)(y - \bar{y}_\varepsilon), \tag{S15}$$

where $(\bar{x}_\varepsilon, \bar{y}_\varepsilon) = \bar{\boldsymbol{x}}_\varepsilon$ is given by (S5). Using the central difference scheme, the discretized version of Eqs. (S14) and (S15) thus read

$$\begin{aligned} &c_1 \frac{u_{i+1,j} - 2u_{i,j} + u_{i-1,j}}{h^2} + c_2 \frac{v_{i+1,j+1} - v_{i+1,j-1} - v_{i-1,j+1} + v_{i-1,j-1}}{4h^2} \\ &+ c_3 \frac{u_{i,j+1} - 2u_{i,j} + u_{i,j-1}}{h^2} = KH_\varepsilon(\varphi^n_{i,j})(x_i - \bar{x}_\varepsilon), \end{aligned} \tag{S16}$$

$$\begin{aligned} &c_3 \frac{v_{i+1,j} - 2v_{i,j} + v_{i-1,j}}{h^2} + c_2 \frac{u_{i+1,j+1} - u_{i+1,j-1} - u_{i-1,j+1} + u_{i-1,j-1}}{4h^2} \\ &+ c_1 \frac{v_{i,j+1} - 2v_{i,j} + v_{i,j-1}}{h^2} = KH_\varepsilon(\varphi^n_{i,j})(y_j - \bar{y}_\varepsilon). \end{aligned} \tag{S17}$$

where $c_1 = \lambda + 2\mu$, $c_2 = \lambda + \mu$, and $c_3 = \mu$.

Discretisation of the evolution law

We first recall the regularised stress $S = (S^{kl})_{2\times 2}$, $1 \le k, l \le 2$, where the entries are given by

$$\begin{aligned} S^{11}(x,y) &= (\lambda + 2\mu)u_x(x,y) + \lambda v_y(x,y), \\ S^{22}(x,y) &= \lambda u_x(x,y) + (\lambda + 2\mu)v_y(x,y), \\ S^{12}(x,y) &= S^{21}(x,y) = (\lambda + \mu)(u_y(x,y) + v_x(x,y)). \end{aligned}$$

We employ the central difference scheme to compute S^{kl}, $1 \le k, l \le 2$. For instance, let S^{11}_{ij} be the numerical approximation to $S^{11}(x_i, y_j)$. Away from the boundaries, we use the central difference to discretize u_x and v_y and get,

$$S^{11}_{ij} = (\lambda + 2\mu)\frac{u_{i+1,j} - u_{i-1,j}}{2h} + \lambda\frac{v_{i,j+1} - v_{i,j-1}}{2h}. \tag{S18}$$

$S^{12}(x,y)$ and $S^{22}(x,y)$ can be discretized in the same way.

At boundaries, to compute S^{kl}, $1 \le k, l \le 2$, we need to impose boundary conditions of u and v. If the Dirichlet boundary conditions are imposed for u and v, we simply use an one-sided finite difference scheme to discretize u_x, u_y, v_x and v_y and compute S^{kl}, since only the stress on the interior domain has contribution to the kinetic relation. When the mixed displacement and traction free conditions are imposed, i.e., $S^{22} = S^{12} = 0$ on the north and south boundary sides (traction free) and $u = v = 0$ on the east and west sides, we discretize u_x, u_y, v_x and v_y using the central difference scheme and eliminate the ghost points (caused by u_y and v_y) through Eqs. (S16), (S17). The corner points are discretized using a first order scheme. Once we get the stress $S = (S^{kl})_{2\times 2}$, we can use (S9) to compute V_n.

Discretisation of the level-set function.

We employ a second-order ENO scheme to discretize (S11), which describes the evolution of the level-set function $\varphi(x,y)$. Since we are interested in the accurately computing the convection of interface position, we use the nonconservative form of the ENO scheme [S5]. Define a minmod function as

$$\text{minmod}(s,t) = \begin{cases} sgn(s)\min(|s|,|t|), & st > 0 \\ 0, & \text{otherwise} \end{cases} \tag{S19}$$

Here sgn means the signum function. (S11) satisfied by the level-set function $\varphi(x,y)$ is a specialized version of the Hamilton-Jacobi equation $\varphi_t - V|\nabla\varphi| = 0$. Given the normal velocity $V = V(x,y,t)$ of the level sets of φ, the second-order ENO discretisation of the Hamilton-Jacobi equation is

$$\varphi^{n+1}_{i,j} = \begin{cases} \varphi^n_{i,j} - \Delta t V^n_{i,j} P_+, & \text{for} V_{i,j} > 0, \\ \varphi^n_{i,j} - \Delta t V^n_{i,j} P_-, & \text{for} V_{i,j} \le 0, \end{cases} \tag{S20}$$

Here we have,

$$
\begin{aligned}
P_+ &= \sqrt{(\max(p_-^x,0)^2+\min(p_+^x,0)^2)+(\max(p_-^y,0)^2+\min(p_+^y,0)^2)},\\
P_- &= \sqrt{(\min(p_-^x,0)^2+\max(p_+^x,0)^2)+(\min(p_-^y,0)^2+\max(p_+^y,0)^2)},\\
p_-^x &= D_-^x\varphi_{i,j}^n + 0.5h\ \text{minmod}(D_-^xD_+^x\varphi_{i,j}^n, D_-^xD_+^x\varphi_{i-1,j}^n),\\
p_+^x &= D_-^x\varphi_{i+1,j}^n - 0.5h\ \text{minmod}(D_-^xD_+^x\varphi_{i+1,j}^n, D_-^xD_+^x\varphi_{i,j}^n),\\
p_-^y &= D_-^y\varphi_{i,j}^n + 0.5h\ \text{minmod}(D_-^yD_+^y\varphi_{i,j}^n, D_-^xD_+^x\varphi_{i,j-1}^n),\\
p_+^y &= D_-^y\varphi_{i,j+1}^n - 0.5h\ \text{minmod}(D_-^yD_+^y\varphi_{i,j+1}^n, D_-^yD_+^y\varphi_{i,j}^n).
\end{aligned}
$$

In practice, even if we prescribe the initial value of the level-set function φ to be a signed distance from the interface, it will not remain so at later times. For large time computations it is desirable to keep φ as a distance function. This will ensure that the interface has a finite thickness of order ε for all time. In [S6], an iterative procedure was proposed to re-initialize φ at each time step, so that it remains a signed distance function from the evolving interface. To be specific, given a level-set function $\varphi^{n+1}(x,y)=\varphi(x,y,t_{n+1})$ at time $t=t_{n+1}$, we compute the solution of the initial-value problem as follows,

$$\Phi_t = sgn(\varphi^{n+1}(x,y))(1-|\nabla\Phi|), \quad (x,y)\in D, \tag{S21}$$

$$\Phi(x,y,0)=\varphi^{n+1}(x,y), \quad (x,y)\in D. \tag{S22}$$

The solution converges rapidly in time to a function that has the same sign and the same zero level set as $\varphi^{n+1}(x,y)$ and also satisfies $|\nabla\Phi|=1$, so that it equals the signed distance from the interface. After φ evolves at each time step according to (S20), it is re-initialized by solving Eqs. (S21) and (S22); this suffices due to rapid convergence. This procedure is crucial for our formulation, since the extension of the normal velocity V in our case is not continuous across the phase boundary in the sharp-interface ε limit. This makes computations more difficult than in the fluid interface problem considered in [S2, S6], where the normal velocity is continuous across the interface.

In our calculations, we use a one-sided finite difference scheme to discretize φ_x and φ_y at the boundary. For example at boundaries $x=-L_x$ and $x=L_x$, $\varphi_x(-L_x,y_j,t_n)$ is approximated by $D_+^x\varphi_{0,j}^n=(\varphi_{1,j}^n-\varphi_{0,j}^n)/h$ and $\varphi_x(L,y_j,t_n)$ is approximated by $D_-^x\varphi_{N,j}^n=(\varphi_{N,j}^n-\varphi_{N-1,j}^n)/h$.

Numerical convergence study.

The minimal mechanosensing model that we have developed is not a standard PDE system (notice that the model consists of coupled PDEs with nonlocal terms) and the zero level set function can develop corners, which bring essential difficulties to a standard rigorous stability analysis. However, the main driving PDE in the model is a level set equation, which is hyperbolic. The method that we used to discretize the level set equation is numerically stable. As such, we perform numerical convergence study to investigate our model's behavior especially in regards to oscillations observed for some parameter values, such as high velocity polarisation $e>2$.

In Fig. S-1, we show the convergence test with respect to the mesh size h. We plot the trajectories of the centroid position and the shape of the cell at final times. We find that both the oscillatory trajectories and the cell shape converge as we refine the mesh size. In Fig. S-2 we show the convergence test with respect to the time step size. We observe similar convergence results for the trajectories of

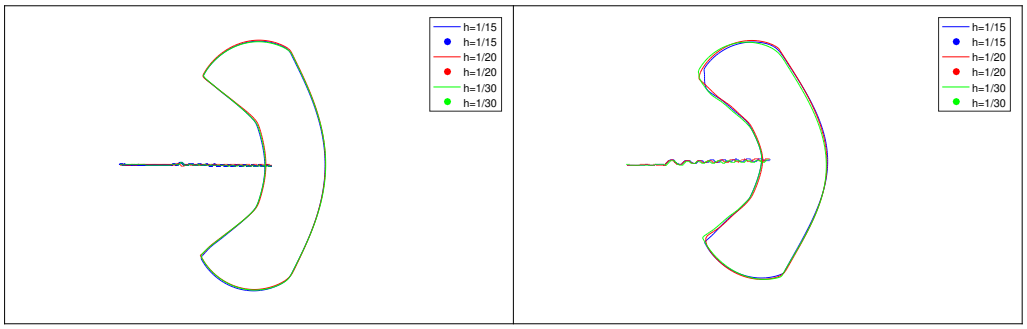

(a) (b)

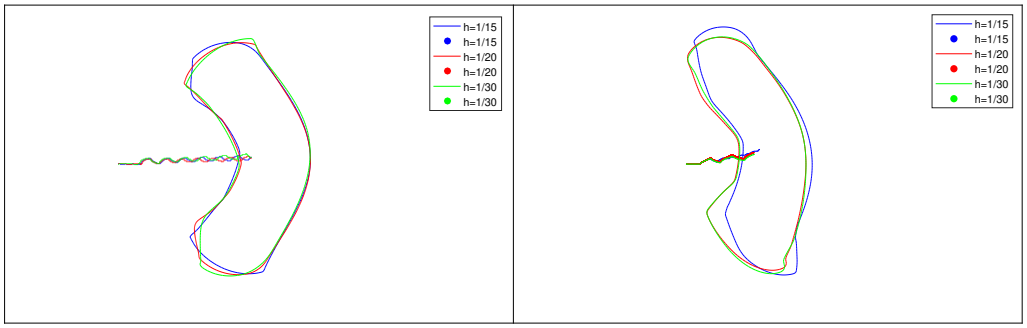

(c) (d)

Figure S-1: Numerical convergence test with respect to the mesh size. (a) $e = 2$. (b) $e = 3$. (c) $e = 5$. (d) $e = 11$. In all three tests, we choose $\Delta t/h = 20$. The computational time for (a)(b)(c) is $t \in [0, 10]$, while the last one is $t \in [0, 8]$. The solid lines are used to show the shape of the cell. The wiggly line is the trajectory of the centroid.

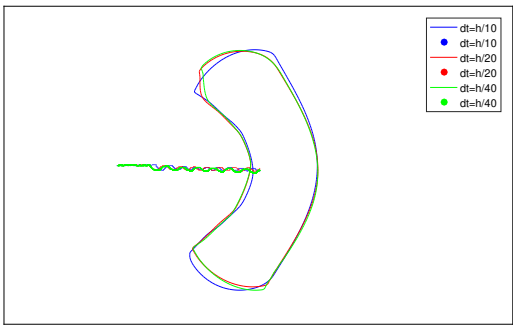

Figure S-2: Numerical convergence test with respect to the time step size. We choose $e = 3$, $h = 1/20$, and computational time $t \in [0, 10]$. The solid lines are used to show the shape of the cell. The wiggly line is the trajectory of the centroid.

the centroid position and the shape of the cell. In our numerical tests, the corresponding Courant-Friedrichs-Lewy (CFL) condition is satisfied. Our numerical results illustrate that oscillations we observed in the bipedal migration arise from the behavior of the model itself, rather than being an artifact of the numerics.

Supplemental Videos

Eight supplemental videos are cited in the main text:

Video SV1.avi

Model simulation of full transition from static annulus to fully developed steady state locomotion in the well-known crescent or banana shape (standard parameters (see Eq.(14) in our paper) except for $e = 1.5$, low polarisation regime.)

Video SV2.avi

Excerpt from Video SV3.avi (standard parameters (see Eq.(14) in our paper) except for $e = 3$, intermediate polarisation regime), with shorter duration but higher time resolution, to show bipedal oscillations.

Video SV3.avi

Model simulation of bipedal oscillatory motion (standard parameters (see Eq.(14) in our paper) except for $e = 3$, intermediate polarisation regime). The displacement field (red arrows) oscillates between symmetry and antisymmetry about the x axis. Note the rather regular oscillatory centroid trajectory with slight deviation from the x axis. (blue curve). Observe upper/lower trailing edges alternating between pointed/rounded and rounded/pointed. shapes, respectively. See also Video SV2.avi

Video SV4.avi

Model simulation of severe irregular oscillations with lamellipodial travelling waves (standard parameters (see Eq.(14) in our paper) except for $e = 11$, high polarisation regime). See also Video SV5.avi

Video SV5.avi

Excerpt from Video SV4.avi (standard parameters (see Eq.(14) in our paper) except for $e = 11$, high polarisation regime), with shorter duration but higher time resolution, to show erratic oscillations and lamellipodial travelling waves (kinks).

Video SV6.avi

Modelling a needle pulling the substrate behind a locomoting cell and away from it (red arrows in ellipse pointing roughly left). The cell turns, moves away transversally to the original direction, elongates toward the needle, then gradually turns toward the needle. Similar behaviour [S7] was recently observed with human epithelial keratinocytes.

Video SV7.avi

Model simulation of durotaxis. A locomoting cell turns toward the top boundary, where zero displacement boundary conditions hold. These are equivalent to an interface with an infinitely stiff region, which attracts the cell.

Video SV8.avi

Model simulation of reverse durotaxis. A locomoting cell turns away from the top boundary, where zero traction boundary conditions hold. These are equivalent to an interface with an infinitely soft region, which repels the cell.

References

[S1] I.S. Sokolnikoff. Mathematical theory of elasticity, Mcgraw-hill book company. *New York*, 1956.

[S2] Y.C. Chang, T.Y. Hou, B. Merriman, and S. Osher. A level set formulation of eulerian interface capturing methods for incompressible fluid flows. *Journal of Computational Physics*, 124(2):449 – 464, 1996.

[S3] Charles W. Wolgemuth and Mark Zajac. The moving boundary node method: A level set-based, finite volume algorithm with applications to cell motility. *Journal of Computational Physics*, 229(19):7287 – 7308, 2010.

[S4] Charles W. Wolgemuth, Jelena Stajic, and Alex Mogilner. Redundant mechanisms for stable cell locomotion revealed by minimal models. *Biophysical Journal*, 101(3):545 – 553, 2011.

[S5] Chi-Wang Shu. Essentially non-oscillatory and weighted essentially non-oscillatory schemes for hyperbolic conservation laws. In *Advanced numerical approximation of nonlinear hyperbolic equations*, pages 325–432. Springer, 1998.

[S6] Mark Sussman, Peter Smereka, and Stanley Osher. A level set approach for computing solutions to incompressible two-phase flow. *Journal of Computational physics*, 114(1):146–159, 1994.

[S7] Hoda Zarkoob, Sathivel Chinnathambi, John C Selby, and Edward A Sander. Substrate deformations induce directed keratinocyte migration. *Journal of The Royal Society Interface*, 15(143):20180133, 2018.